Antireflective Coating Nanocrystalline α-Fe₂O₃ Layer for Solar Cell Applications

Marwa Fathy[1]✎, Ahmed I. Omran[2], Waheed A. Badway[2]

[1]Electronic Materials Department Advanced Technology and New Materials Research Institute, City of Scientific Research and Technology Applications (SRTA-City), New Borg El-Arab City, P.O. Box 21934, Alexandria, Egypt
[2] Chemistry Department, Faculty of Science, Cairo University

Abstract: A new antireflective nano-coating of α-Fe₂O₃ for glass surfaces using dip-coating technique working in the visible and near infrared optical spectrum was developed and characterized. α-Fe₂O₃ nanoparticles were synthesized by hydrothermal process. Thermal transformation strategy is designed to transfer β-FeOOH into α-Fe₂O₃. The structure and morphology of the iron oxide nanoparticles were analyzed by XRD, FTIR, and SEM. Optical properties of antireflective coatings (ARC) deposited from ethanolic solution of α-Fe₂O₃ have been characterized. 93.4 % optical transmittance using optimal dip coating conditions (dipping rate – 3 cm/10 sec, coating time – 5min, and temperature – 25 ºC) for annealed powder at 300 °C for 1 hr.

Keywords: Antireflective coating; α-Fe₂O₃; dip coating; optical properties

1. Introduction

Antireflective coatings (ARC) are widely used for reflectance minimization in numerous applications, such as flat panel displays [1,2], organic light-emitting diodes (OLEDs) [3], thin-film solar cells [4,5], lasers, and all kinds of lenses [6]. In the cases of flat panel displays and OLEDs, the AR films are deposited on the glass substrates to suppress Fresnel reflection at the air-glass interface [7].

A key issue in preparing the AR coating is the formation of large area, and uniform layer. Different self-assembly processes can be in principle used to achieve this goal, such as spin coating [8,9], dip coating [10,11], layer-by-layer assembly [12,13], soft lithography [14,15], and evaporation-induced self-assembly [16].

Weakly-ferromagnetic α-Fe₂O₃ (hematite) is of particular interest as a cheap, environmentally friendly and thermodynamically stable iron oxide [17]. Synthetic hematite (α-Fe₂O₃) has been extensively used in the field of pigments [18], catalysts [19], magnetic materials [20], anticorrosive agents [21] and sensors [22], owning to its low cost, environmental friendliness, and high resistance to corrosion [23]. The synthesis of iron oxides nanocrystals of different size and shape has attracted considerable interesting in recent years [24].

In the present study, we demonstrated the preparation of nanocrystaline α-Fe₂O₃ as AR coating on lime glass substrates by dip-coating technique and showed the dependence of variation of the AR behavior on different deposition process parameters and heat treatment.

2. Materials and methods
2.1. Materials

Iron(III) chloride (FeCl₃ anhydrous, 98%) was obtained from Acros organics company (Geel, Belgium). hydrochloric acid (HCl) and ethanol absolute (C₂H₅OH) were purchased from Fisher chemical company. All chemical reagents utilized as received without further purification.

2.2. Method

The α-Fe₂O₃ hydrosol was synthesized by using hydrolysis method as the raw material and its thin films were deposited on glass substrates by dip coating technique. Predetermined amounts of stock solutions of FeCl₃ and HCl were mixed in a flask at the ratio of 1:3 (v/v), and the deionized water was added till the final concentration of Fe^{+3} is 0.01 M. This mixture was preserved in water bath at 90 °C for 24 hrs, and then cooled to room temperature. The resulting orange-red solution was centrifuged (6000 rpm for 15 mins) and dried at 60°C overnight on vacuum oven.
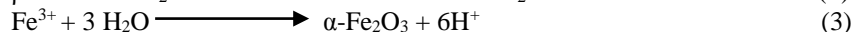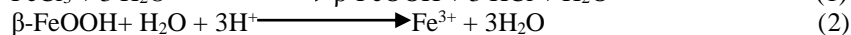
✎ **Marwa Fathy (Correspondence)**
✉ mrwfathy@gmail.com, **mfathy@mucsat.sci.eg**
☎ +203 4593414, Fax: +203 4593414

The overall hydrolysis reactions were illustrated in Equations 1-3 [25].

$$FeCl_3 + 3 H_2O \longrightarrow \beta\text{-FeOOH} + 3 HCl + H_2O \qquad (1)$$
$$\beta\text{-FeOOH} + H_2O + 3H^+ \longrightarrow Fe^{3+} + 3H_2O \qquad (2)$$
$$Fe^{3+} + 3 H_2O \longrightarrow \alpha\text{-Fe}_2O_3 + 6H^+ \qquad (3)$$

The as-prepared powder was annealed at 300 ℃ and 500 ℃ for 1h. After annealing, red powder was produced. Thin films of S1, S2, and S3 samples were deposited on soda-lime glass substrates using dip-coating technique (As mentioned in Table 1). The dip coating solutions were prepared by dissolve the produced powders in 50 mL absolute ethanol.

Table 1: powder and thin films samples

	Powder sample		**Dip coating sample (thin film on two side of glass substrate)**	
S1	As-prepared	**S1L**		0.025 g/50 ml ethanol
S2	Annealed at 300 ˚C for 1 hr	**S2L**	**S2LA**	0.025 g/50 ml ethanol
			S2LB	0.05 g/50 ml ethanol
S3	Annealed at 500 ˚C for 1 hr	**S3L**		0.025g/50 ml ethanol

2.3. Characterizations

X-ray powder diffraction (XRD) patterns were obtained using X-Ray diffractometer (Schimadzu 7000, Japan), operating with Cu Kα radiation (λ=0.154060 nm). Fourier transform infrared (FT-IR) spectra were recorded on a Shimadzu FTIR- 8400 S (Japan) transform infrared spectrometer in the region of 400–4000 cm^{-1} using KBr pellets.

Scanning electron microscopy (SEM) measurements were performed used a JEOL, JSM-6360 LA to examine the morphology and the homogeneity of the surface.

Optical transmittance was measured covering the spectral regions from 190 nm to 1100 nm with a standard UV–Vis double beam PC scanning spectrophotometer (LABOMED, INC).

4. Results and Discussion
4.1. Structural analysis

Fig. 1 showed the X-ray diffraction (XRD) patterns of the β-FeOOH prepared by hydrothermal process and the α-Fe$_2$O$_3$ product obtained after annealing process [27]. For S1 sample, it cauld be seen that, the peaks at 2θ of 26.7°, 33.4°, 35.2°, 39.2°, 46.23°, 48.89°, 56 °, 62.3°, and 64.2°, were assigned to (310), (400), (211), (301), (411), (141), (060), (002), and (112) lattice planes of orthorhombic β-FeOOH phase, respectively (according to card number 00-018-0639).

But some week peaks of rhombohedral α-Fe$_2$O$_3$ appeared at 39.2°, 43.6°, 54.09°, 56°, 62.3°, and 67.02° were assigned to (006), (202), (116), (211), (214), and (125). The great mass of the diffraction peaks could be indexed to the standard β-FeOOH.

The crystallite size can be determined from the broadening of corresponding X-ray spectral peaks by Scherrer formula (Equation 4)[26].

$$L = K \lambda / (\beta \cos \theta) \qquad (4)$$

Where L is the crystallite size, λ is the wavelength of the X-ray radiation (Cu Kaα =0.15418 nm), K is usually taken as 0.89, and β is the line width at half-maximum height, after subtraction of equipment broadening.

The calculated crystallite size of S2 and S3 had the value of 30.1 nm and 61.94 nm, respectively.

This result could be explained according to the growth rate Equation 5 which given by [27]:

$$u = a_0 v_0 [\exp(-Q/KT)][1-\exp(-\Delta F_v/KT)] \qquad (5)$$

where a_0 is the particle diameter, v_0 is the atomic jump frequency, Q is the activation energy for an atom to leave the matrix and attach itself to the growing phase, and ΔF_v the molar free energy difference between the two phases.

For non-crystallization, $\Delta F_v \gg KT$, so Equation (5) can be reduced to [28]:

$$u = a_0 v_0 [\exp (-Q/KT)] \qquad (6)$$

The crystallite size increases with increasing the heat treatment temperature.

For S2 sample, it was found that, the β-FeOOH precursor was converted into a pure rhombohedral structure of α-Fe$_2$O$_3$ (according to card number 00-033-0664) after annealing process at 300 ˚C for 1 hr. Diffraction peaks of α-Fe$_2$O$_3$ were observed but with low intensity. No other diffraction peaks were observed, indicating that no impurity existed and the β-FeOOH completely transformed into the α-Fe$_2$O$_3$. S3 sample, all peaks of α-Fe$_2$O$_3$ were appeared with

high intensity at 24.13°, 33.2°, 35.6°, 39.4°, 40.8°, 43.52°, 49.4°, 54.1°, 57.2°, 62.4°, 64°, and 69.5° which are assigned to (012), (104), (110), (006), (113), (202), (024), (116), (122), (214), and (300), respectively (according to card number 00-033-0664).
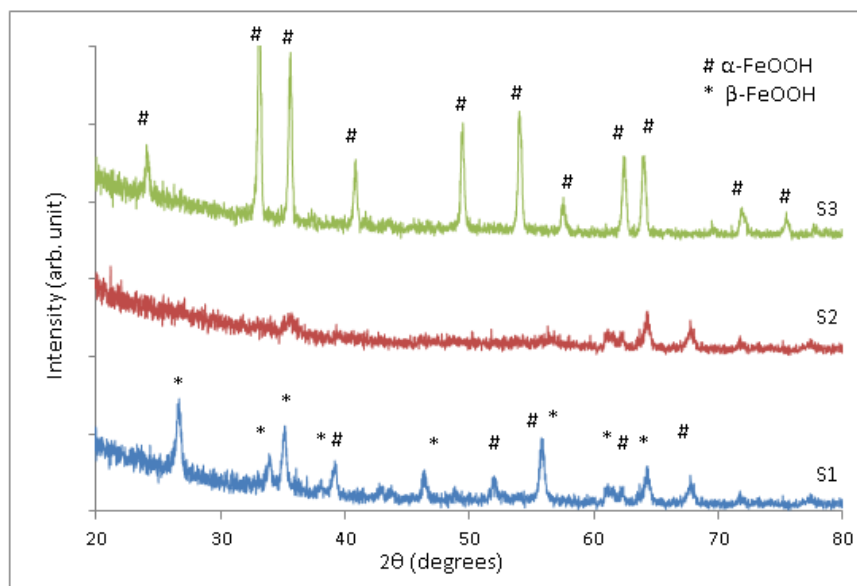

Fig. 1. XRD patterns of S1, S2, and S3 powder samples.

Fig. 2 presented FTIR spectra obtained from S1, S2, and S3.

It was clear that the signals from S3 were relatively strong compared to S1 and S2. The FTIR spectrum of S1 showed characteristic vibrations of H_2O and Fe-OH bands. A broad bands 3340 and 1626 cm^{-1} were assigned to O-H and H-O-H bending vibrations of β-FeOOH and H_2O. Also, the bands at 644 and 862 cm^{-1} were assigned to Fe-O vibrational mode of β-FeOOH. The experimental results demonstrated that β-FeOOH was obtained as a result of the hydrothermal interaction between $FeCl_3$ with HCl. After annealing process at 300 ˚C for 1 hr (S2), FTIR broad bands of S1 were weakened. Also, two new weak bands at 578, 447 cm^{-1} were appeared which characteristic of α-Fe₂O₃ spheres [29].

Increasing the annealing temperature into 500 ˚C (S3), these two peaks at 3420 and 1640 cm^{-1} were completely disappeared. The sharp bands at 575 and 485 cm^{-1} were observed. The FTIR results indicate the formation of α-Fe₂O₃ in the present experiment after annealing process at 300 ˚C and 500 ˚C for 1 hr, which are consistent with the XRD result [30].
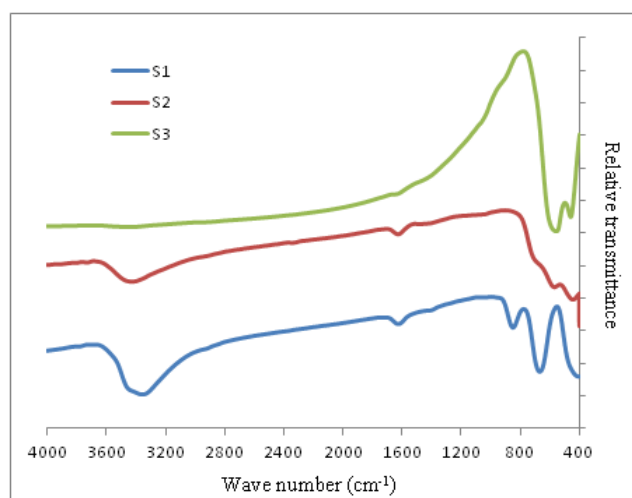

Fig. 2. FTIR spectra of S1, S2, and S3 samples.

4.2. Morphological analysis

Fig. 3 illustrated the SEM images of the as prepared nano-powder and annealed samples (S1), (S2) and (S3). For S1, very small spindle or elongated particles were produced with size range of 55-65 nm, demonstrating the increase of the overall dimension relative to β-FeOOH [31]. When the as-prepared powder was annealed at 300 ˚C for 1h (S2), irregular spherical grains of α-Fe$_2$O$_3$ nano-particles with diameter of 100-150 nm was appeared. When the annealing temperature was increased to 500 ˚C for 1hr (S3), the particles were aggregated with each other and form spherical grains with large a diameter 500 nm.

4.3. Optical analysis

Table 2 showed the direct optical transmittance of S2LA, and S2LB samples without and with heat treatment at 200 ˚C for 15 min. Also the effect of immersing time of glass substrate on the dip-coating solution was demonstrated. It was found that, the heat treated sample with immersing time of 5 mins was given higher transmittance than untreated samples. It means that, using of low concentration of α-Fe$_2$O$_3$ ethanolic solution increase the transparency of the film and the heat treatment remove any impurities and enhance the adhesion of the material on the substrate.
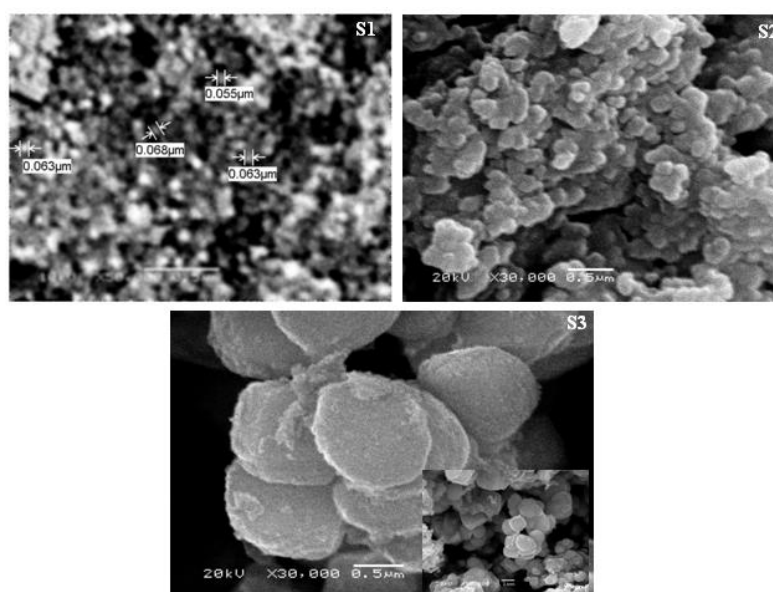

Fig. 3. SEM of S1, S2, and S3 samples.

Table 2. Effect of solution concentration on the optical transmission of samples without and with heat treatment at 200 C for 15 min

Sample Immersing interval		S2LA (T%)	S2LB (T%)
3 min	Without HT	91.9	91.1
	With HT	92.8	92.8
5 min	Without HT	92.1	91.8
	With HT	92.9	**93**

Table 3 showed the effect of number of layers deposited on glass substrate. The direct transmittance was enhanced in the whole spectrum for AR film deposited with one layer and dipping for 5 min with heat treatment sample compared to that of the bare glass as shown in Fig. 4.

Table 3. Effect of immersing interval and number of layers on the optical transmission of samples without and with heat treatment at 200 ˚C for 15 min

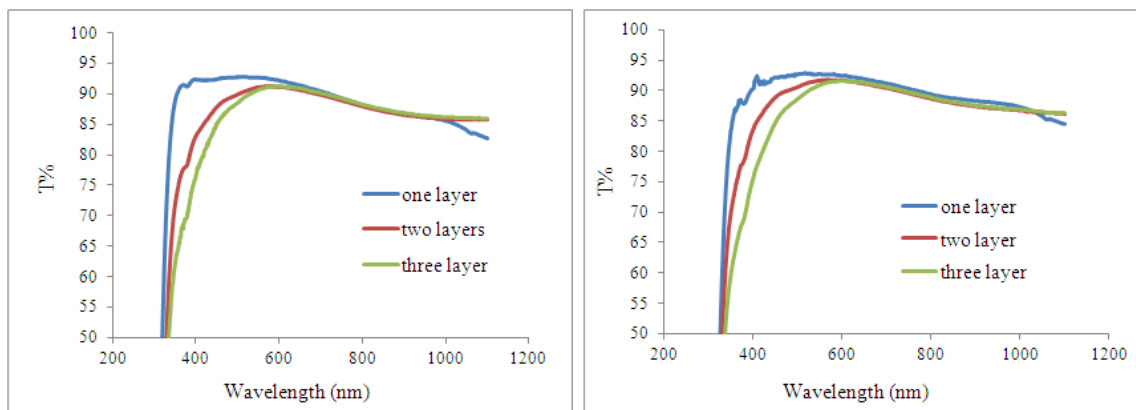| No. of layer (S2LA) / Immersing interval		One layer (T%)	Two layer (T%)	Three layer (T%)
3 min	Without HT	91.3	91.5	90.7
	With HT	92.7	91.3	91.2
5 min	Without HT	91.7	91.8	90.5
	With HT	**92.9**	91.4	91.7

Fig. 4. Optical transmittance spectra of S2LA thin films with different number of layers deposited on glass substrates with immersing interval 3 min (left) and 5 min (right).

The optical transmittance of films deposited on glass substrates using powder samples S1, S2, and S3 were presented in Table 4 and shown in Fig. 5. It was found that, the morphology of the samples has a great effect on the transmittance of the samples. For elongated particles of β-FeOOH in S1L and the large grains of α-Fe$_2$O$_3$ in S3L caused reflection or scattering for the light which incident on the samples which lead to reduce in the whole transmittance value of the films[32].

Table 4. Effect of heat treatment at 300˚C and 500˚C for 1hr on the optical transmittance of AR films

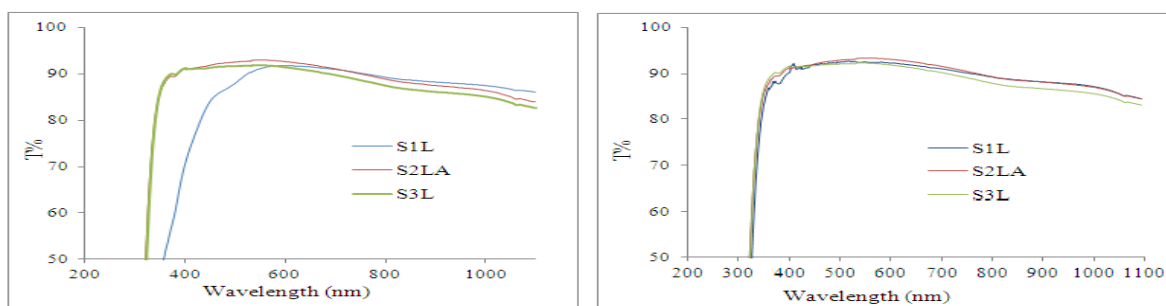| Samples / Immersing interval		S1L (T%)	S2LA (T%)	S3L(T%)
5 min	Without HT	91.8	93.0	91.9
	With HT	92.9	**93.4**	92.4

Fig. 5. Optical transmittance spectra of thin films of S1L, S2LA, and S3L samples; without (left) and with HT (right).

4. Conclusions

Nanocrystalline iron oxide (III) has been prepared by hydrothermal method. orthorhombic β-FeOOH phase was produced after hydrothermal process. After annealing at high temperature (300 ˚C), rhombohedral α-Fe$_2$O$_3$ was obtained. Increasing the annealing temperature into 500˚C lead to increase the crystallinity of the produced α-Fe$_2$O$_3$ nanoparticles with crystallite size of 30 nm. For antireflective coating of nanocrystalline α-Fe$_2$O$_3$ layer on soda lime glass substrates deposited by dip-coating technique (dipping rate – 3 cm/10 sec, coating time – 5min, and temperature – 25 ℃), the maximum optical transmittance was 93.4 % for annealed powder at 300 °C for 1 hr.

5. References

1- Joo W, Kim Y, Jang S, Kim JK. Antireflection coating with enhanced anti-scratch property from nanoporous block copolymer template, Thin Solid Films, 2011; 519: 3804–3808.
2- Min WL, Jiang B, Jiang P, Bioinspired self-cleaning antireflection coatings", Adv. Mater., 2008;20: 3914–3918.
3- Li Y, Li F, Zhang J, Wang C, Zhu S, Yu H, Wang Z, Yang B, Improved light extraction efficiency of white organic light-emitting devices by biomimetic antireflective surfaces, Appl. Phys. Lett. 2010;96: 153305-153307.
4- Kuo ML, Poxson DJ, Kim YS, Mont FW, Kim JK, Schubert EF, Lin SY, Realization of a near-perfect antireflection coating for silicon solar energy utilization, Opt. Lett. 2008;33: 2527–2529.
5- Raut HK, Ganesh VA, Nair AS, Ramakrishna S, Anti-reflective coatings: a critical, in-depth review, Energy Environ. Sci. 2011;4: 3779–3804.
6- Mu Q, Li Y, Wang H, Zhang Q, Self-organized TiO$_2$ nanorod arrays on glass substrate for self-cleaning antireflection coatings, Colloid and Interface Science, 2012;365: 308–313.
7- Lu Y, Zhang X, Huang J, Li J, Wei T, Lan P, Yang Y, Xu H, Song W, Investigation on antireflection coatings for Al:ZnO in silicon thin film solar cells, International Journal for Light and Electron Optics, 2013;124: 3392–3395.
8- Biswas PK, Devi PS, Chakraborty PK, Chatterjee A, Ganguli D, Kamath MP, Joshi AS, Porous anti-reflective silica coatings with a high spectral coverage by sol–gel spin coating technique, J. Mater. Sci. Lett. 2003;22: 181–183.
9- Zhang QY, Wang J, Wu G, Shen J, Buddhudu S, Interference coating by hydrophobic aerogel-like SiO$_2$ thin films, Mater. Chem. Phys., 2001;72: 56–59.
10- Nostell P, Roos A, Karlsson B, Optical and mechanical properties of sol–gel antirefective films for solar energy applications, Thin Solid Films 1999;351: 170–175.
11- Uhlmann DR, Suratwala T, Davidson K, Boulton JM, Teowee G, Sol–gel derived coatings on glass, J. Non-Cryst. Solids, 1997;218: 113–122.
12- Hiller J, Mendelsohn JD, Rubner MF, Reversibly erasable nanoporous anti-reflection coatings from polyelectrolyte multilayers, Nat. Mater. 2002;1: 59–63.
13- Rouse JH, Ferguson GS, Preparation of thin silica films with controlled thickness and tunable refractive index, J. Am. Chem. Soc. 2003;125: 15529–15536.

14- Koo, HY, Yi, DK, Yoo, SJ, Kim, DY, A snowman-like array of colloidal dimmers for antireflecting surfaces, Adv. Mater., 2004;16: 274-277.
15- Chen HL, Chuang SY, Lin YH, Using colloidal lithography to fabricate and optimize sub–wavelength pyramidal and honeycomb structures in solar cells, Opt. Express, 2007;15: 14793–14803 .
16- Dimitrov AS, Miwa T, Nagayama K, "A comparison between the optical properties of amorphous and crystalline monolayers of silica particles, Langmuir 1999;15: 5257–5264.
17- Almeida TP, Fay M W, Zhu YQ, Brown PD, Process map for the hydrothermal synthesis of α-Fe$_2$O$_3$ nanorods, J. Physical Chemistry C, 2009;113: 18689-18698.
18- Guskos N, Papadopoulos GJ, Likodimos V, Patapis S, Yarmis D, Przepiera A, Majszczyk J, Typek J, Wabia M, Aidinis K, Drazek Z, Photoacoustic, EPR and electrical conductivity investigation of three synthetic mineral pigments: hematite, goethite and magnetite, Mater. Res. Bull., 2002;37: 1051-1061.
19- Liu H, Wei Y, Sun Y, Preparation of lepidocrocites with different degrees of crystallization and their photocatalytic properties, J. Mol, Catal, A: Chem. 2005;226: 135–140.
20- Brice-Profeta S, Arrio MA, Tronc E, Menguy N, Letard I, Cartier dit Moulin C, Nogue`s M, Chaneac C, Jolivet JP, Sainctavit Ph. Magnetic order in γ-Fe$_2$O$_3$ nanoparticles : a XMCD study, J. Magnetism and Magnetic Materials 2005;288: 354–365.
21- Bondioli F, Ferrari AM, Leonelli C, Manfredini T, Monoferrite BaFe$_2$O$_4$ applied as ceramic pigment CMDM, Mater. Res. Bull. 1998;32: 723–729.
22- Pelino M, Colella C, Cantalini C, Faccio M, Ferri G, D'Amico A, "Strontium-doped hematite as possible humidity sensing material for soil water content determination, Sens. Actuat. B: Chem. 1992;7: 464–469 .
23- Flynn Jr, CM, Photochemistry of hydrolytic iron (III) species and photoinduced degradation of organic compound, Chem. Rev. 1984;84: 31–41.
24- Wang X, Ammonium mediated hydrothermal synthesis of nanostructured hematite (α-Fe$_2$O$_3$) particles", Materials Research Bulletin 2012;47: 2513–2517.
25- Almeida T, Hydrothermal synthesis and characterisation of α-Fe$_2$O$_3$ nanorods, Doctoral Thesis, University of Nottingham, (2010).
26- Uvarov V, Popov I, Metrological characterization of x-ray diffraction methods for determination of crystallite size in nano-scale materials, Materials Characterization, 2007;58: 883–891.
27- Li B, Wang X, Yan M, Li L, Preparation and characterization of nano-TiO$_2$ powder, Materials Chemistry and Physics, 2002;78: 184–188.
28- Kashyout AB, Soliman M, Fathy M, Effect of preparation parameter on the properties of TiO$_2$ nanoparicles for dye sensitized solar cells, Renewable Energy 2010;35: 2914-2920.
29- Sun P, You L, Wang D, Sun Y, Ma J, Lu G, Synthesis and gas sensing properties of bundle-like α-Fe$_2$O$_3$ nanorods, Sensors and Actuators B 2011;156: 368–374.
30- Ristic M, Music S, Godec M, Properties of γ-FeOOH, α-FeOOH and α-Fe$_2$O$_3$ particles precipitated by hydrolysis of Fe^{3+} ions in perchlorate containing aqueous solutions, J. Alloys and Compounds, 2006;417: 292–299.
31- Wang F, Qin XF, Meng YF, Guo ZL, Yang LX, Ming YF, Hydrothermal synthesis and characterization of α-Fe$_2$O$_3$ nanoparticles, Materials Science in Semiconductor Processing, 2013;16: 802–806.
32- Song H, Zhang X, Chen T, Jia X, One-pot Synthesis of Bundle-like β-FeOOH Nanorods and their Transformation to Porous α-Fe$_2$O$_3$ Microspheres, Ceramics International, 2014;40: 15595-15602.